

Capillary electroosmosis properties of water lubricants with different electroosmotic additives under a steel-on-steel sliding interface

Bohua FENG¹, Zhiqiang LUAN¹, Tao ZHANG¹, Jiawei LIU¹, Xiaodong HU¹, Jiju GUAN², Xuefeng XU^{1,*}

¹ Key Laboratory of Special Purpose Equipment and Advanced Manufacturing Technology, Ministry of Education & Zhejiang Province, Zhejiang University of Technology, Hangzhou 310023, China

² College of Mechanical Engineering, Changshu Institute of Technology, Changshu 215500, China

Received: 15 May 2020 / Revised: 09 September 2020 / Accepted: 14 March 2021

© The author(s) 2021.

Abstract: The process of lubricant penetration into frictional interfaces has not been fully established, hence compromising their tribological performance. In this study, the penetration characteristics of deionized water (DI water) containing an electroosmotic suppressant (cetyltrimethylammonium bromide (CTAB)) and an electroosmotic promoter (sodium lauriminodipropionate (SLI)), were investigated using steel-on-steel friction pairs. The results indicated that the lubricant with electroosmotic promoter reduced the coefficient of friction and wear scar diameter, whereas that with an electroosmotic suppressant exhibited an opposite behavior compared with DI water. The addition of SLI promoted the penetration of the DI water solution, thus resulting in the formation of a thick lubricating film of iron oxide at the sliding surface. This effectively reduced the abrasion damage, leading to a lower coefficient of friction and wear loss.

Keywords: electroosmosis; friction interface; electroosmotic additives; water lubricants; tribological performance

1 Introduction

In mechanical systems, lubricants are widely used to reduce friction and improve worn surface quality [1]. During cutting processes, lubricants can enter contact surfaces to form lubricating films through the gaps at the tool–chip interface, which generates a film-to-film contact of low shearing resistance and hence improves interfacial friction and wear conditions. Nevertheless, the penetration mechanism of lubricants into the interface of frictional pairs is still not well understood, thus compromising their cutting performance. Previous studies [2–4] pointed out that capillaries exist at the contact interface of two sliding pairs, such as tool–workpiece interfaces and the contact surfaces of friction pairs, and lubricants

thus penetrate the contact zone through these capillaries. In recent years, various transparent tools have been designed and used in the machining of pure lead, aluminum, and copper to study the penetration mechanism of lubricants [5, 6]. The experimental results showed that during machining, capillaries were indeed formed at the end of the tool–chip interface. Many of authors [3, 5] believed that these capillaries play a critical role in lubricant penetration. These capillaries serve as passageways by which lubricants can enter and wet the contact interface and promote the formation of lubricating films. Bieria et al. [7] found that lubricants were driven to the tool–chip interface via these microscale capillaries under both capillary force and atmospheric pressure for lubrication. The study reported in Ref. [8]

* Corresponding author: Xuefeng XU, E-mail: xuxuefeng@zjut.edu.cn

demonstrated that the penetration depth of lubricants into capillaries was directly proportional to the coefficient of the capillary force in the liquids but inversely proportional to the capillary radius. The pressure formed within the capillaries was also verified to be the main driving force in the lubricant penetration process [9]. Xu et al. [10] studied the effects of capillary force, atmospheric pressure, and capillary wall viscous resistance on the penetration performance of cutting fluids during grinding of Cr12 die steel. Their results showed that the capillary penetration depth of grinding fluids was a complex process dominated by multiple forces. Thus, the process and mechanism of lubricant penetration into frictional interfaces need to be further clarified.

During the friction and wear processes, the contact interface of frictional pairs is broken, scratched, or undergoes plastic deformation. The highly active "fresh" surface is exfoliated, and the electrons overflow from these "fresh" surfaces, leading to electron emission [11], which mainly includes chemi-emission [12], fracto-emission [13, 14], and tribo-emission [15]. Govindaraj and Subbiah [16] observed electron emission during the cutting process of stainless steel, low carbon steel, and copper using carbide tools with different cutting parameters. They pointed out that the magnitude of the electron emission was not only related to the resistivity, hardness, tensile strength, and yield strength of the material, but also to the cutting speed and depth. The electron emission intensity accumulated for 1,000 ms during scratching of a carbon film with a diamond stylus under dry air condition was approximately 100 pC [17]. The magnitudes of the electron emission and tribo-electrification intensity for metal–metal contact are inferior to those between insulators and semiconductors [18], however, it was shown that tens of microvolts could still be generated between friction pairs made of Fe/Fe [19]. The emitted electrons are affected by a strong normal electric field at the friction interface, causing a gas discharge in the gap of the friction pair that generates a plasma [20] under dry friction [21] or oil-lubricated [22] conditions. These triboelectric phenomena can generate a self-excited electric field at the friction interface, which may generate

an electrokinetic effect on the lubricants in the capillaries, promoting the penetration of lubricants through capillary electroosmosis.

Capillary electroosmosis is a process in which the electrolyte solution in a capillary moves relative to the fixed wall of the capillary under an applied electric field. The capillary, axial electric fields at both ends of the capillary, and electrical double layer (EDL, including the diffusion layer and fixed layer) produced at the liquid/solid interface are the necessary factors for capillary electroosmosis [23]. The walls of metals, quartz, and most natural substances are negatively charged when they are immersed in a water-based solution [24]. The formation of the EDL is mainly due to the resulting surface charge of the capillary wall. Co-ions from the solution are repelled and counter-ions are attracted to screen the surface charges, creating a charged region close to the capillary inner surface [25]. Because of the strong electrostatic effect between ions, the fixed layer ions are immobilized, whereas the diffusion layer ions move under the effect of the electric field. The movement of diffusion layer ions drives the solution in the capillary to move concurrently under the influence of the solution viscosity and finally forms an electroosmotic flow (EOF) [26]. In general, the EOF can be promoted by enhancing the electric field strength [27], increasing the pH [28], and reducing the internal diameter of the capillaries [29]. Moreover, zwitterionic surfactants [30] (such as 3-[(3-cholamidopropyl)-dimethylammonio]-1-propanesulfonate (CHAPS) and sodium lauriminodipropionate (SLI)) can improve the EOF, but cationic surfactants [31] (such as cetyltrimethylammonium bromide (CTAB) and tetradecyltrimethylammonium bromide (TTAB)) may change the EOF direction [29] due to a change in the EDL properties caused by the adsorption of electroosmotic additive molecules on the capillary surface. Chen et al. [32] systematically studied the application of a high-pressure electroosmotic pump in micro-column liquid chromatography and designed an electroosmotic pump with an output pressure of at least 5 MPa and a stable flow rate of about 1 $\mu\text{L}/\text{min}$ for pure water and methanol. They reported that the EOF rate and pressure could be controlled quantitatively by adjusting the

driving voltage at both ends of the capillary and the diameter of the capillary. Wang and Wu [33] investigated the driving characteristics of microfluids on a moving wall. They pointed out that an increase in the moving speed of the wall could improve the EOF speed and rate when the fluid pressure in the micro-channel and the driving voltage were constant. Zhong and Chen [34] found that the EOF velocity of deionized (DI) water was approximately 11 mm/s when an electric field of 800 V/cm was applied to both ends of a capillary with a diameter of 25 μm . This result was similar to that (approximately 3.55 mm/s) of an investigation based on a capillary penetration model of the tool–chip contact zone [9].

In this study, we first developed a device for measuring the EOF velocity of DI water with two types of electroosmotic additives at various concentrations. Second, the tribological performances of DI water with the electroosmotic additives were evaluated by four-ball tests of steel-on-steel contact pairs to explore the penetration characteristics of lubricants in the capillaries of the friction interface. Third, we also investigated the effects of different rotational speeds and applied loads on the friction and wear properties when taking the capillary electroosmosis effect in the friction interface into consideration. Finally, X-ray photoelectron spectroscopy (XPS) of the worn surfaces lubricated by DI water with different electroosmotic additives was conducted. The goal of this study is to explore the penetrability of lubricants at steel-on-steel friction interfaces and reveal the mechanism of electroosmosis, which affects the capillary penetration of lubricants at the friction interface.

2 Methods

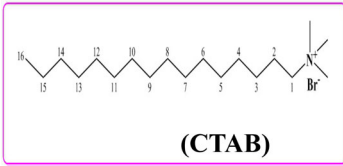
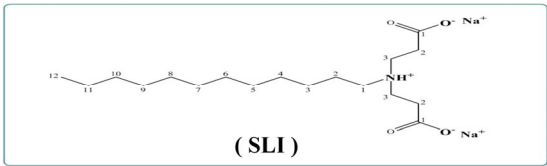
2.1 Preparation of the lubricants

To minimize the influence of excess ions in the lubricating fluid on these exploratory experiment, DI water was used as the reference lubricant because of its simple composition and its positive and negative ions due to hydrolysis of water molecules [35]. In this study, CTAB (cationic surfactant) and SLI (zwitterionic surfactant) were used as electroosmotic additives, and DI water was employed as the base fluid. Electroosmotic additives in powder form were directly added into the base fluid at a concentration range of 0.05–0.3 mM (mmol/L). Subsequently, the lubricants were ultrasonically treated in a water bath for 30 min to ensure complete dissolution of the electroosmotic additives. Both electroosmotic additives were purchased from Shanghai Macklir Biochemical Co., Ltd., China. DI water containing CTAB was used as the electroosmotic suppressant lubricant, and DI water containing SLI was used as the electroosmotic promoter lubricant. The main properties of the electroosmotic additives used are summarized in Table 1.

2.2 Capillary electroosmosis experiment

The surface tension and contact angle of the lubricants utilized in this study were measured by the drop weight method [36] and goniometry method [37], respectively. Each group of experiments was repeated five times at room temperature, and the average value was recorded. To measure the EOF velocity of the various lubricants under different conditions, a

Table 1 Properties of the electroosmotic additives.

| Electroosmotic additives | CTAB | SLI |
|----------------------------|--|--|
| Function | Electroosmotic suppressant | Electroosmotic promoter |
| Relative molecular mass | 364.5 | 373.44 |
| Physical state | Powder | Powder |
| Chemical molecular formula |  <p style="text-align: center;">(CTAB)</p> |  <p style="text-align: center;">(SLI)</p> |

device, as shown in Fig. 1, was fabricated. The capillaries used in the device were 304 stainless steel tubes with internal/external diameters of 0.5/1.1 mm and 0.9/1.5 mm, and a length of 40 mm. Syringes of 2.5 mL were vertically installed on both sides of the device. After fabricating the device, ultrasonic cleaning with DI water for 10 min was performed to ensure tidiness of the inner wall of the capillaries and syringes. The lubricants were added from one side of the syringe to avoid bubbles, and the two sides of the liquid level in the syringe were finally in horizontal position under the action of gravity. Each type of lubricants was added to the 1.5 mL level of both syringes. The electrodes in contact with the lubricants were platinum electrodes with a diameter of 2 mm. The output end of the high-voltage electrostatic generator (EST802A, Beijing Huajinghui Technology Ltd., China) was connected to the left electrode with an output voltage of 1.5 kV or 3 kV, whereas the other electrode was grounded. According to the formula $E=U/d$, the intensities of the electric field generated at both ends of the capillary were approximately 400 V/cm and 800 V/cm, which exceeded the starting electric field intensity of capillary electroosmosis (150 V/cm) [38]. Each test lasted for 30 min, and the EOF velocities of the different lubricants were calculated based on their moving volume. Each test was repeated

five times at room temperature (25 °C), and the average value was then recorded.

2.3 Friction and wear testing

The tribological tests were conducted on an MMW-1 multispecimen test system (Jinan Shijin Group-Co., Ltd., China). The tribological properties of the lubricants containing CTAB and SLI were compared with those of pure DI water under different testing conditions using a four-ball method (see Fig. 2(a)). The test conditions were as follows: at room temperature (25 °C); additive concentrations of 0.05, 0.1, 0.2, and 0.3 mM; rotational speeds of 600, 800, 1,000, and 1,200 rpm; and loads of 49, 98, and 147 N. The evaluation duration was 30 min. The steel balls employed in the tests were 12.7 mm in diameter and made of AISI 52100 steel with an HRC hardness of 59–61. The scratches on the friction interface shown in Fig. 2(b) were a half cylinder with a radius of $\sim 1 \mu\text{m}$. As a counterpart ball slid on it, a cylinder cavity was formed, which was approximately considered to be a capillary [1, 39, 40]. The change in the experimental parameters affected the morphology of the capillaries on the friction interface, thus influencing the penetration effect of the lubricants [5, 41]. Figure 2(c) presents a schematic of the friction capillary interface. A

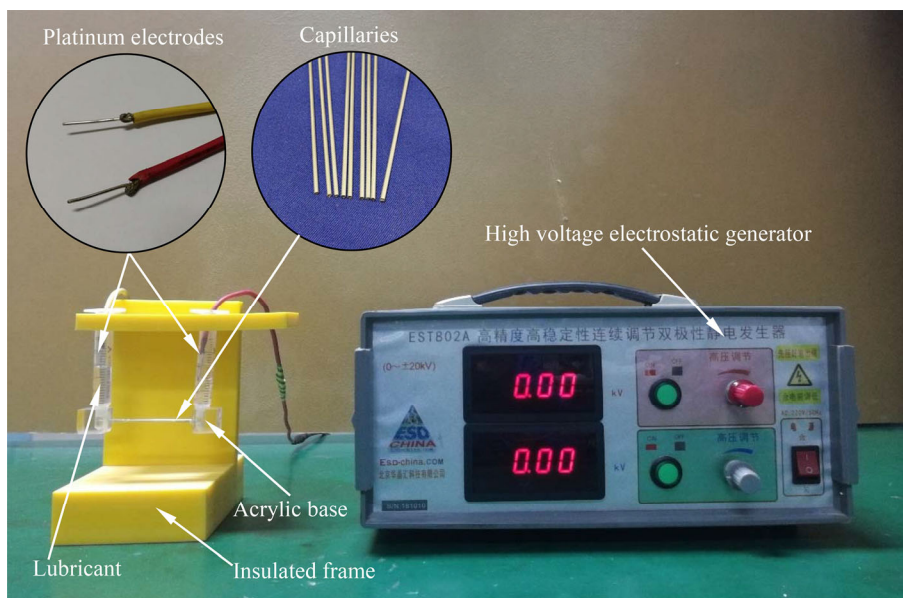


Fig. 1 Photograph of the device designed for measuring the EOF velocity of the lubricants.

strong radial electric field was generated due to the frictional electrification between the friction surfaces [19, 42], and the electrons emitted from the sliding contact were affected by this electric field, which generated a plasma [20, 22]. These above phenomena resulted in an axial self-excited electric field directed toward the closed end in the capillary. To analyze the chemical states and distribution of the chemical elements on the worn surfaces, additional ball-on-disk tests were performed. The steel balls used for these tests were the same as those for the four-ball tests, and the steel disks employed were $\phi 32 \text{ mm} \times \phi 16 \text{ mm} \times 0.8 \text{ mm}$. They were made of AISI 52100 steel with an HRC hardness of 25–28. The tests were conducted at room temperature (25 °C), an additive concentration of 0.2 mM, a rotational speed of 800 rpm, and a load of 98 N; the test duration was 15 min. Before testing, the specimen holders and test balls/disks were dipped in acetone and cleaned in an ultrasonic bath for 10 min. Each test was repeated five times, and the average value was recorded. After each test, the disks and balls were cleaned in an ultrasonic bath. The wear scar diameters (WSDs) of the balls and the surface topographies of the disks were analyzed using a three-dimensional dynamic microscope system (VW-6000, Keyence, Japan). The worn surfaces of the balls and disks were examined using a scanning electron microscopy (SEM) system equipped with an

energy dispersive X-ray spectroscopy (EDS) (EVO18, Zeiss, Germany), and a Kratos AXIS Ultra DLD X-ray photoelectron spectrometer (Shimadzu Corporation, Japan) equipped with an Al $k\alpha$ radiation source (15 keV, 10 mA). The pass energy was 20 eV for fine scanning at a resolution of 0.3 eV, using the binding energy of adventitious carbon (284.8 eV) as a reference.

3 Results and discussion

3.1 Capillary electroosmosis properties

Due to the diameter limitation of commercial capillaries, it is difficult to investigate the electroosmosis properties of lubricants in small capillaries with an internal diameter of 1–2 μm [9]. Therefore, macroscopic capillaries with different diameters were used to comparatively investigate the EOF velocity of different solutions. Table 2 presents the measurements of the surface tensions and contact angles of DI water and lubricants with the two different surfactants, in which the results of the DI water were used as a comparison. We observed that the surface tensions and contact angles of the two kinds of lubricants were smaller than those of the DI water and decreased with increasing surfactant concentration. The EOF velocities of the lubricants containing CTAB and SLI under different conditions are depicted in Figs. 3(a) and

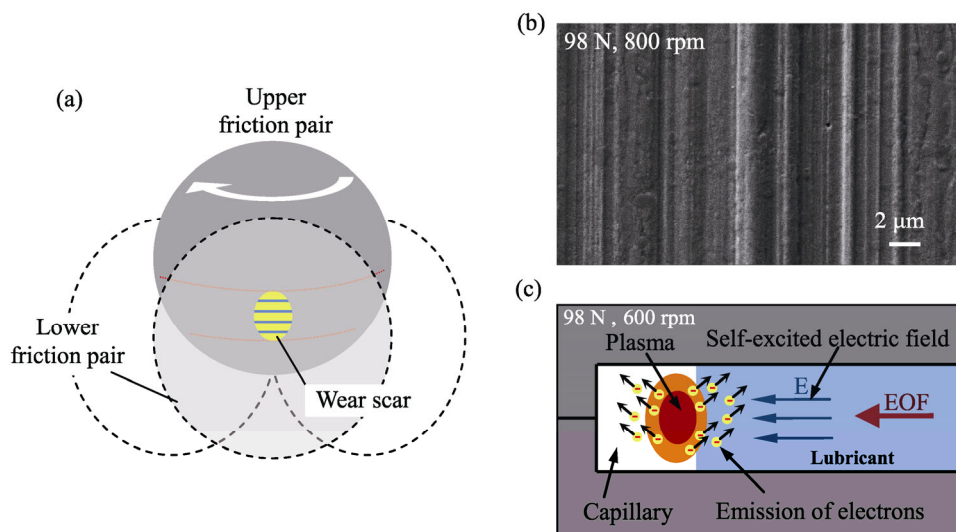


Fig. 2 (a) Schematic of the four-ball test. (b) Capillaries at the friction interface. (c) Schematic of the friction capillary interface.

3(b). The absolute values of the EOF velocities of both lubricants increased rapidly with the increase in CTAB and SLI concentrations under the same electric field strength. With an increase in the electric field intensity on both sides of the capillary, the absolute values of both EOF velocities increased obviously. For example, the EOF velocities of DI water in the capillary with an internal diameter of 0.9 mm were 0.65×10^{-4} and 0.77×10^{-4} $\mu\text{L}/\text{ms}$ when the electric field intensities were 400 and 800 V/cm, respectively. It should also be noted that the EOF velocity increased with a decrease in the inner diameter of the capillary. The EOF velocities of the DI water under 800 V/cm in the capillaries with internal diameters of 0.5 and 0.9 mm were 1.09×10^{-4} and 0.77×10^{-4} $\mu\text{L}/\text{ms}$, respectively. This is mainly because the increased ratio of the side area to the cross-sectional area of the capillary can improve the EOF [29]. The maximum absolute values of the EOF velocities were recorded when the concentrations of CTAB and SLI reached 0.2 and 0.1 mM, respectively. This may be because the adsorption of electroosmotic additives molecules in the inner surface of the capillary tended to become saturated [43, 44].

As shown in Fig. 3, the direction of the EOF velocity is opposite to that of the electric field when CTAB lubricants are employed. This is mainly because the quaternary ammonium cationic group of the CTAB molecule is positively charged [45], and the CTAB molecules are firmly adsorbed on the inner wall of the capillary under the influence of the electrostatic attraction [46]. With the increase in CTAB concentration, the adsorption quantity of the CTAB molecules on the capillary wall increased gradually until the entire negatively charged internal wall of the capillary was covered, forming a single molecule adsorption layer. The density of negative charges on the capillary wall continued to decrease until it reached zero, and the EOF weakened until it disappeared eventually.

The second adsorption layer on the capillary walls was formed by the interaction of the hydrophobic chains in the CTAB molecules with the increased concentration of CTAB, as displayed in Fig. 4(a). Chen [38] suggested that when the CTAB concentration in the solution reaches 0.05 mM, the second

adsorption layer forms (at this time, the direction of the EOF begins to reverse). With the increase in CTAB concentration, the rate of the reversed EOF increased. When the CTAB concentration reached 0.2 mM, the velocity of the EOF became stable, and the adsorption of CTAB molecules on the inner surface of the capillary reached saturation.

Additionally, we can observe from Fig. 3 that the direction of the EOF velocity is the same as that of the electric field when SLI lubricants are used. Under 400 V/cm, the EOF velocities of the SLI lubricant with 0.2 mM were 36.9% and 29.6% higher than those of the DI water with capillary inner diameters of 0.5 and 0.9 mm, respectively. Under 800 V/cm, the enhancing effect of the SLI lubricant with 0.2 mM on the EOF was stronger: the velocities were 54.5% and 36.7% higher than those of DI water, respectively. A possible reason for this phenomenon is that one SLI molecule has one cationic group containing nitrogen and two carboxylic acid anion groups. As shown in Fig. 4(b), the positive cationic groups of the SLI molecules are closely adsorbed on the negatively charged capillary walls and form an additional fixed layer under the electrostatic effect between the charges. The carboxylic acid anion groups remained in the solution and did not move with the movement of the solution. This condition doubled the negative charge on the capillary wall, resulting in the enhanced EOF [47].

Upon combining Table 2 with Fig. 3, it can be seen that when the surfactant concentration increased from 0.2 to 0.3 mM, although the surface tension and contact angle continued to decrease, the EOF velocity did not change significantly. This result indicates that the penetration of the lubricating fluid in the capillaries was mainly controlled by the EOF instead of electrowetting at such a low concentration of surfactant.

3.2 Tribological properties

3.2.1 Tribological behaviors under different concentrations

Figure 5 presents the variations in COF and WSD as a function of concentration when the lubricants containing CTAB and SLI are used. The performance

Table 2 Values of the contact angles and surface tensions for the three Different types of lubricants at various concentrations. The results achieved by DI water were used for comparison.

| Lubricant | | Surface tension γ (mN·m ⁻¹) | Contact angle θ (°) |
|-----------|----------|---|-------------------------------|
| 0 mM | DI water | 72.0 | 79.5 |
| 0.05 mM | CTAB | 60.9 | 77.7 |
| | SLI | 61.7 | 77.3 |
| 0.1 mM | CTAB | 58.3 | 75.6 |
| | SLI | 60.1 | 76.1 |
| 0.2 mM | CTAB | 57.1 | 74.1 |
| | SLI | 58.2 | 74.3 |
| 0.3 mM | CTAB | 54.9 | 72.1 |
| | SLI | 55.9 | 71.5 |

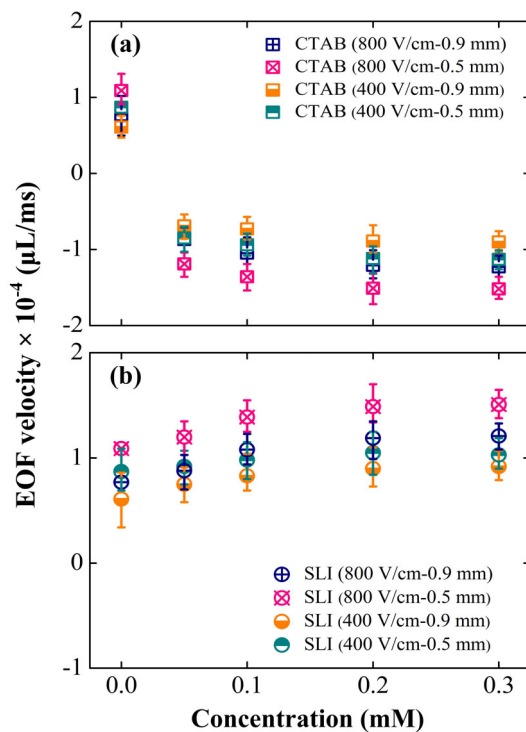


Fig. 3 Effect of electroosmotic additive type and concentration, capillary diameter, and electric field strength on EOF velocity. The values consistent with the direction of the electric field line are positive, and the test time is 30 minutes. The types of electroosmotic additives are (a) CTAB and (b) SLI.

achieved using DI water is also shown in Fig. 5 for comparison. The COFs and WSDs increased with increasing concentration of CTAB, and the highest friction increase was obtained when the concentration of CTAB reached 0.2 mM. The COF and WSD were

25.5% and 10.4% higher compared with those of DI water (0.289 in COF and 0.692 mm in WSD), respectively. This could be because CTAB might suppress the penetration of lubricants into the friction interface due to the changed EDL structure on the inner walls of the capillary, reducing the amount of lubricants participating in the anti-friction and anti-wear processes and consequently increasing the COF and WSD.

As illustrated in Fig. 5, the COFs and WSDs sharply decrease and then remain stable with increasing concentrations of SLI. When the concentration of SLI reached 0.1 mM, the best performance was recorded, in which the COF and WSD were 22.7% and 10.7% lower than those of DI water, respectively. These results suggest that the addition of SLI promotes the EOF toward the deeper friction interface, leading to more lubricants entering into the capillaries of the friction interface to participate in the anti-wear process, resulting in the reduction of the COF and WSD. However, when the concentration of electroosmotic additives continued to increase, the COFs and WSDs basically remain unchanged. This should be due to the saturation of the adsorption of CTAB and SLI molecules on the inner wall of the capillary [48].

Figure 6 displays the SEM images and EDS spectra of the worn surfaces of the friction balls under different lubrication conditions. In Fig. 6(a), a large number of deep furrows are clearly shown on the worn surface employing the CTAB lubricant, indicating severe abrasive wear. However, the furrows produced by the SLI lubricant were shallower, as presented in Fig. 6(c), suggesting a better anti-wear capacity. The EDS spectra detected within the dashed boxed areas on the worn surfaces show that the contents of Br on the worn surfaces are 0 wt%, and those of the Na element are 0.01–0.09 wt%. CTAB contains Br while SLI contains Na, suggesting that only very small amounts of the additives were involved in the lubrication process during the trials. In addition, the maximum mass fractions of CTAB and SLI in the electroosmotic suppressant lubricant and electroosmotic promoter lubricant are only 0.0109 wt% and 0.0112 wt%, respectively. Therefore, the lubricating performances

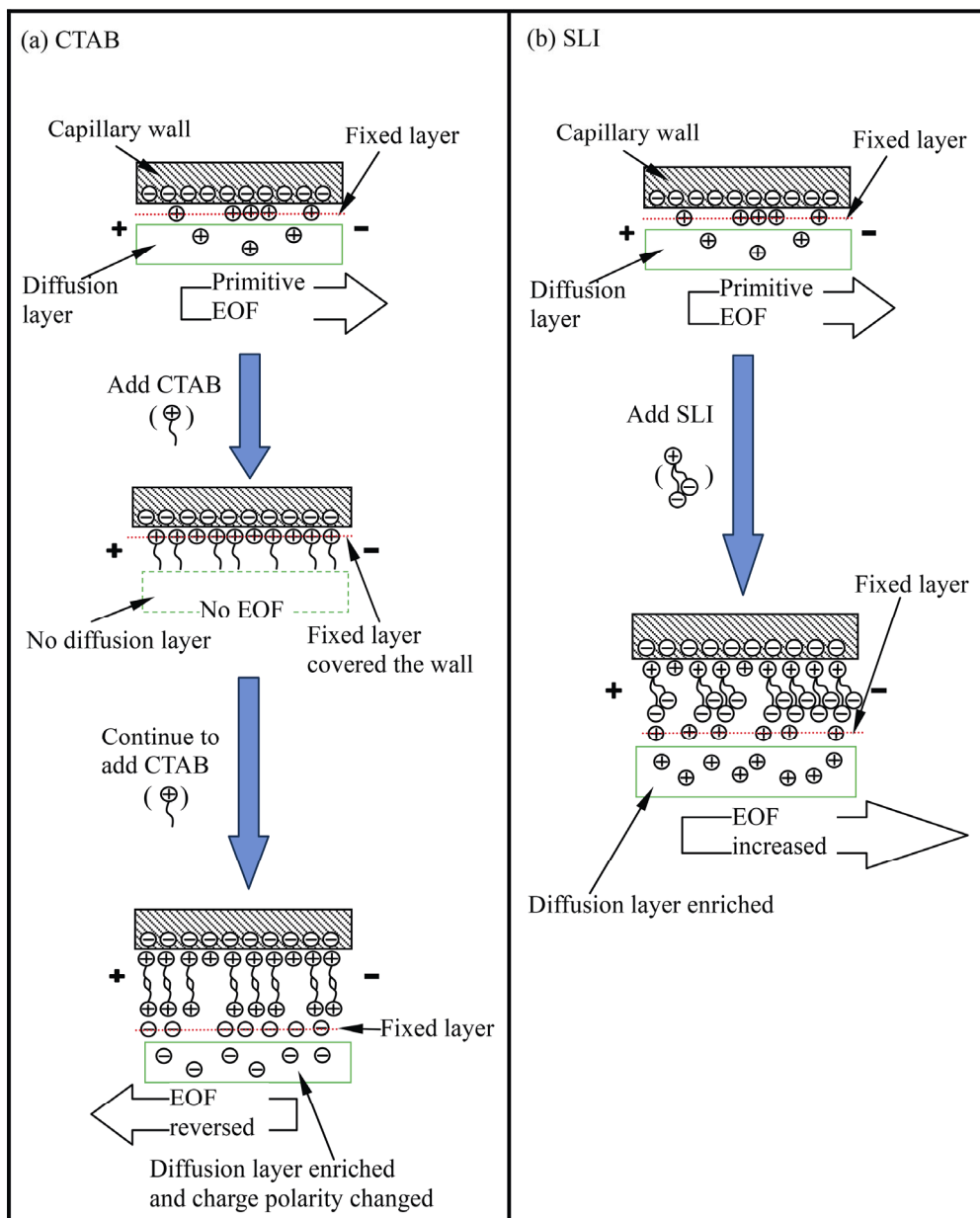


Fig. 4 Regulation mechanism of different electroosmotic additive molecules on EOF: (a) CTAB and (b) SLI.

of the electroosmotic additives themselves had little effect on the anti-friction and anti-wear performance of the lubricants. The improvement in the tribological performance of the lubricant may be mainly due to the amount of lubricant penetrating into the steel-on-steel sliding interface. In addition, the content of O on the worn surface using the SLI lubricant is higher than that of the other two cases, indicating that more oxygen is supplied to participate in the anti-wear process and form an oxide film on the worn surface. Additional details

are discussed in Section 3.3.

3.2.2 Tribological behavior under different rotational speeds

Figure 7 shows the WSD and COF as a function of rotational speed under the lubrication conditions of the electroosmotic suppressant and electroosmotic promoter; the results recorded under DI water are used for comparison. The COFs decreased rapidly, whereas the WSDs showed an opposite trend with increasing rotational speed. Huang et al. [49] found

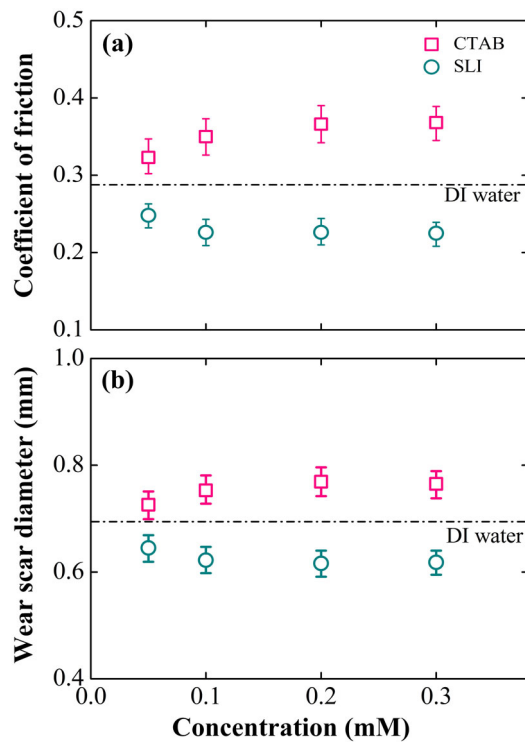


Fig. 5 Effect of electroosmotic additive concentration on (a) COFs and (b) WSDs for four-ball tests at 800 rpm and 98 N. The results obtained using DI water are used for comparison.

that the variations in the COF and wear rate of friction pairs were closely related to the contact condition of the friction pairs with varying sliding speed when they compared the anti-wear performance under minimum quantity lubrication (MQL) and electrostatic minimum quantity lubrication (EMQL) conditions at different test speeds. As indicated in Fig. 7, the COFs and WSDs lubricated by the SLI lubricant are comparatively lower than those lubricated by the CTAB lubricant at all rotational speeds. Compared with DI water (0.289), the use of SLI and CTAB lubricants could achieve a 22.5% reduction but a 25.5% increment in COF, respectively, when the rotational speed was 800 rpm. This may be mainly because the increase in rotating speed could result in severer contact, which increases the axial electric field strength at both ends of the capillary at the friction interface. The addition of SLI can promote more water and oxygen molecules penetrating the friction interface, which promote the formation of an oxide film, thus enhancing the tribological performance. However, the addition of CTAB suppresses the penetration of water into

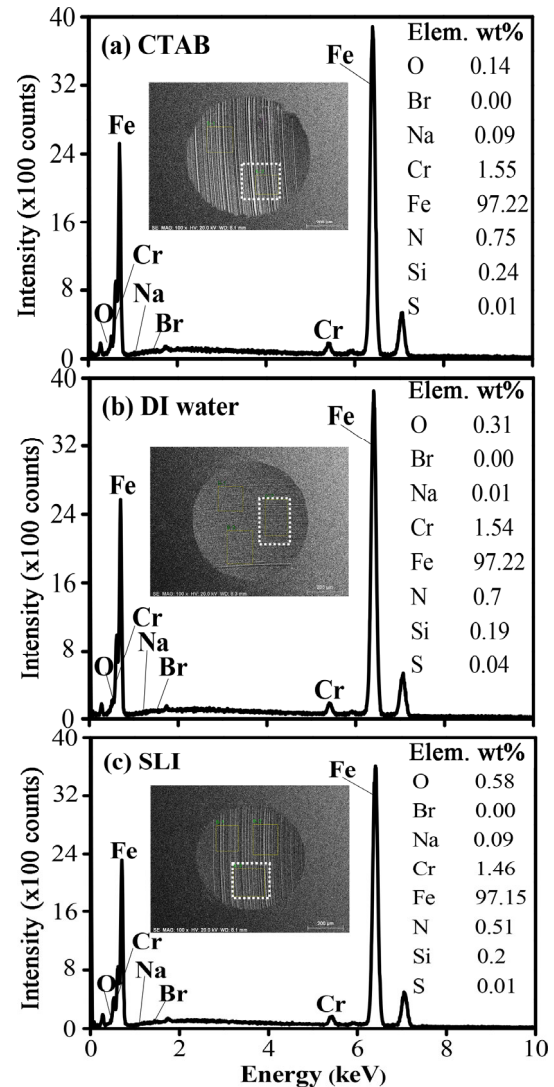


Fig. 6 SEM images of the worn surfaces lubricated with (a) CTAB, (b) DI water, and (c) SLI, and EDS spectra detected at the dashed boxed areas on the worn surfaces of the SEM images at 0.2 mM electroosmotic additive concentration, 800 rpm, and 98 N.

the friction interface, leading to a worse tribological performance.

3.2.3 Tribological behaviors under different applied loads

Figure 8 depicts the COF and WSD as a function of the applied load under different lubrication conditions using the results recorded under DI water as comparison. The COFs and WSDs of the SLI lubricant are lower than those of the CTAB lubricant under different loads. The capability of SLI in promoting the lubricant into the capillaries of the

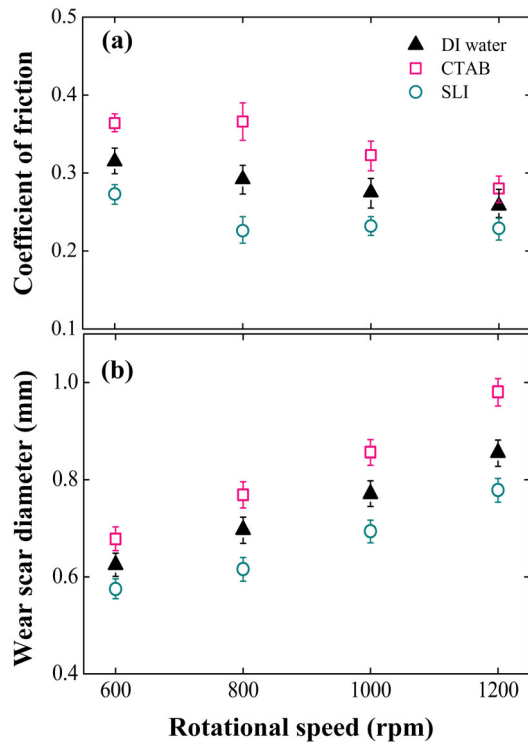


Fig. 7 Effect of rotational speed on (a) COFs and (b) WSDs for four-ball tests at 0.2 mM electroosmotic additive concentration and 98 N.

friction interface is remarkable based on the reduced COFs and WSDs in comparison with CTAB. As can be seen from Fig. 8, the COF initially decreases and then increases with increasing applied load for both SLI lubricant and DI water cases. It is possible that the increase in the applied load leads to an increase in wear surface roughness, leading to the increase in the diameter of the capillaries on the worn surface, resulting in a lower EOF [40]. As explained earlier, the axial electric fields at both ends of the capillary were enhanced by the production of a strong plasma in the friction zone when the applied load increased. A stronger electric field accelerates the EOF of lubricants and promotes lubricant penetration into the contact interface. Moreover, it can bring more oxygen molecules into the contact area to form an anti-wear layer, thus achieving a better tribological performance [16]. However, when the load is further increased, the excessive pressure between the friction pairs may cause the anti-wear layer formed on the worn surface to peel off quickly [50], increasing the wear of the friction pairs, as reflected by the larger values of COF.

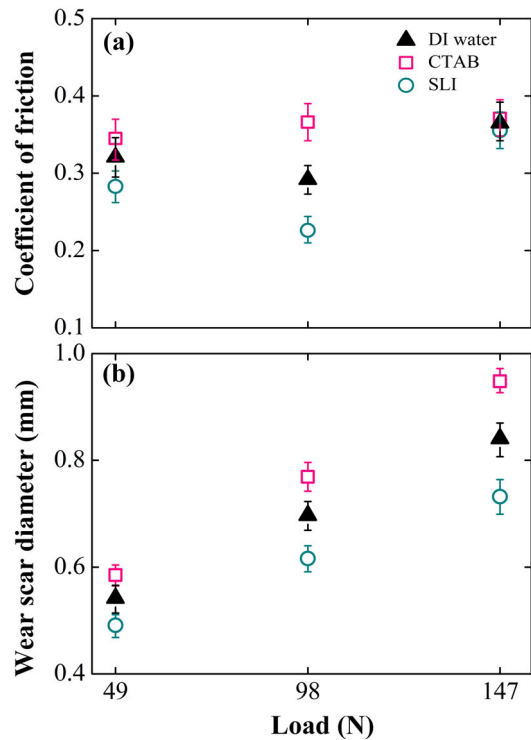


Fig. 8 Effect of applied load on (a) COFs and (b) WSDs for four-ball tests at 0.2 mM electroosmotic additive concentration and 800 rpm.

3.2.4 Surface topography

Figure 9 compares the overall characteristics of the SEM and optical micrographs of the worn surfaces under all conditions. It is evident from Figs. 9(a, c, e) that the quality of the worn surfaces using the SLI lubricant was better than those using the DI water and CTAB lubricants, which is consistent with the relevant friction and wear behaviors. A possible explanation for this result may be that more lubricant penetrated the interface of the friction pair and formed an oxide layer on the worn surface. The oxide layer could effectively protect the worn surface of the friction pairs and minimize scratches, leading to a better surface quality. Regarding the experimental evidence on the SEM micrographs shown in Figs. 9(b, d, f), typical characteristics of irregular lamellar wear debris are clearly obtained on the surfaces in all cases. Moreover, even flake shedding occurred under the DI water and CTAB lubrication conditions, which demonstrated that adhesion and plastic deformation took place [51]. In addition, there are plowing

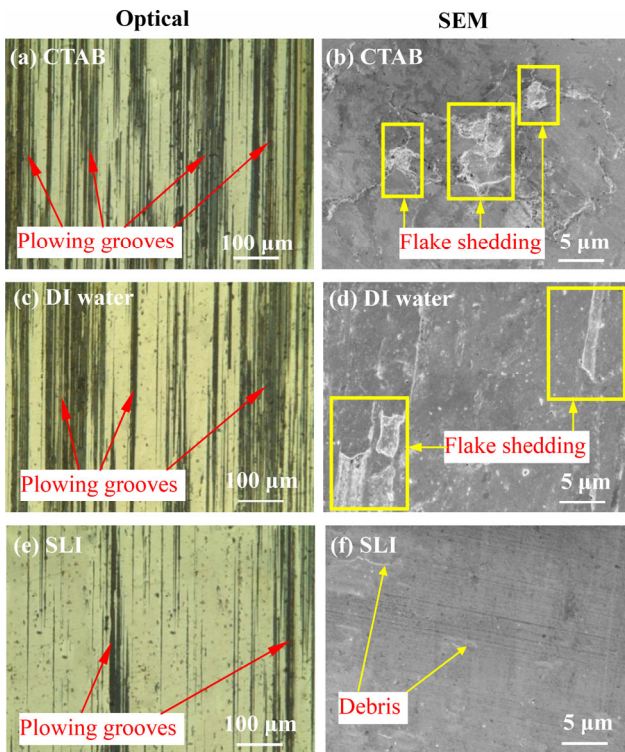


Fig. 9 Optical and SEM micrographs of the worn surfaces lubricated with (a, b) CTAB lubricant, (c, d) DI water, and (e, f) SLI lubricant at 0.2 mM concentration, 800 rpm, and 98 N.

grooves with different degrees on the worn surfaces under all lubrication conditions. Therefore, it appears that the wear mechanism for all lubricants is generally dominated by the combination of adhesive wear, abrasive wear, and plastic deformation.

3.3 XPS analysis of worn surfaces

To investigate the effect of the electroosmotic additives on the penetrability of the lubricating fluid at the friction interface, the worn disk surfaces were analyzed by XPS. Figure 10 provides the O 1s and Fe 2p XPS spectra on the raw AISI 52100 steel and worn surfaces lubricated by the CTAB, SLI, and DI water lubricants. XPSPEAK 41 was employed to fit the spectral elements, and Table 3 lists the relative areas of FeO, Fe₂O₃ and Fe₃O₄, and FeOOH on the AISI 52100 steel and worn surfaces.

For the AISI 52100 steel surface, the peaks in the O 1s spectra illustrated in Fig. 10(a) are related to the absorbed Fe–O bonds. The 710.7 and 725.1 eV binding energies, probed in the Fe 2p spectrum

presented in Fig. 10(b), are attributed to Fe 2p_{3/2} and Fe 2p_{1/2} for Fe₂O₃ and Fe₃O₄, but the 706.8 eV binding energy may be assigned to Fe 2p_{3/2} for Fe [37]. Furthermore, the peak at ~719.7 should be ascribed to the satellite peak of Fe 2p_{3/2} for Fe₂O₃ and Fe₃O₄ [52].

For the DI water lubrication condition, new peaks are detected in the Fe 2p spectra, as shown in Fig. 10(b). The ~712.7 eV binding energy is attributed to the Fe 2p_{3/2} for FeOOH, indicating that there is a chemical reaction between DI water and Fe at the friction interface [53]. In addition, the peaks at 709.9 and 724.1 eV are attributed to the Fe 2p_{3/2} and Fe 2p_{1/2} for FeO [36]. According to the observations above, we can infer that an oxide layer is formed on the contact interface with DI water lubrication.

For the CTAB lubricant, the respective peaks at 531.2 eV and ~712.7 eV correspond to the FeOOH also existing on the O 1s and Fe 2p spectra. Compared with that by DI water, the peaks assigned to the Fe 2p_{3/2} and Fe 2p_{1/2} for FeO obviously weakened, and the relative areas of FeOOH in addition to Fe₂O₃ and Fe₃O₄ detected on the worn surface produced with the CTAB lubricant are lower than those of DI water (see Table 3). This indicates that only a preliminary chemical reaction took place on the worn surface and the oxide film formed on the worn surface was thin. This is because the CTAB molecules formed a second adsorption layer on the capillary wall under the action of the electrostatic force between charges, reducing the EOF and causing less lubricating fluid to participate in the anti-wear process.

For the SLI lubricant, the types of peaks detected on the worn surface are the same as those of DI water. However, the relative areas of FeOOH and Fe₂O₃&Fe₃O₄ detected on the worn surface produced by the SLI lubricant are higher than those of DI water (see Table 3). This demonstrated that the penetrating capacity of the lubricants into the contact interface was improved when the electroosmotic promoter was employed, and more oxygen was supplied to produce an oxide film on the worn surface [9]. The existence of a higher oxygen content on the worn disc surface caused the Fe⁰ and Fe²⁺ to

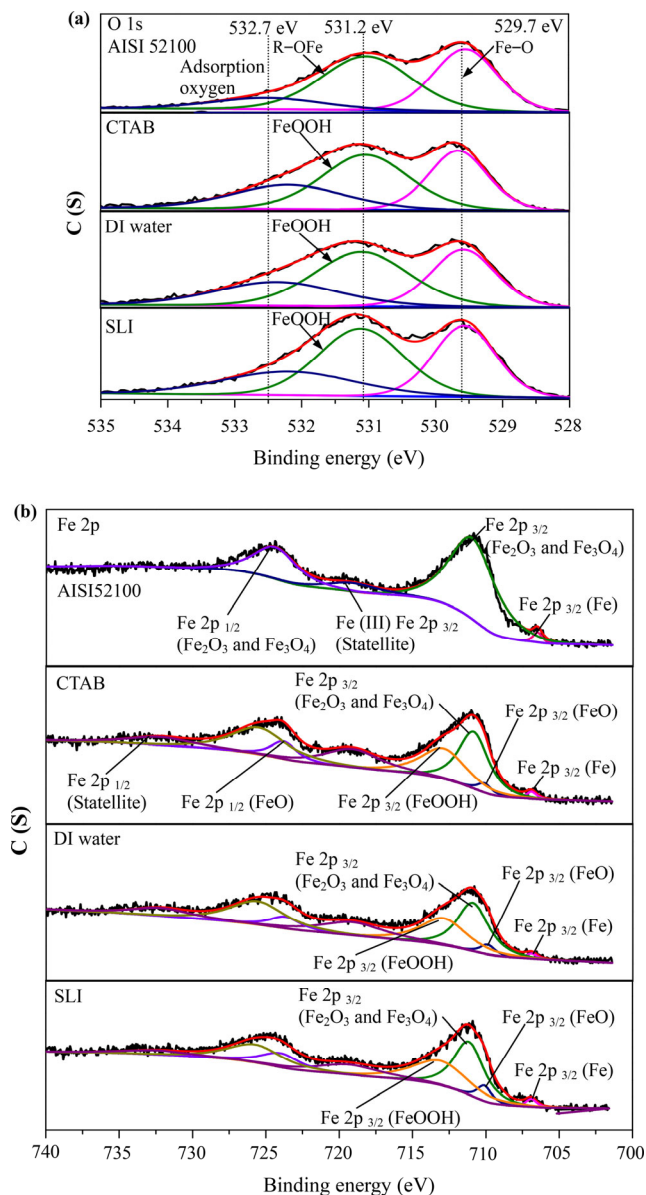


Fig. 10 XPS spectra of (a) O 1s and (b) Fe 2p on the AISI 52100 steel surface and the worn surfaces lubricated with CTAB, DI water, and SLI lubricants.

transform into Fe^{3+} [52].

Based on the above findings, a penetration model of the friction region under different lubricants is illustrated in Fig. 11. The penetration property of DI water into the capillaries of the friction interfaces differed under the addition of different electroosmotic additives, leading to a different thickness oxide film generated on the friction interfaces, which consisted of Fe_2O_3 & Fe_3O_4 and FeOOH . The contact on the friction interface was changed from steel on steel to film on film owing to

Table 3 Relative areas of FeO , Fe_2O_3 and Fe_3O_4 , and FeOOH on AISI 52100 steel and worn surfaces produced using the CTAB, DI water, and SLI lubricants.

| | Relative area (%) | | |
|------------|-------------------|---|-------|
| | FeO | Fe_2O_3 and Fe_3O_4 | FeOOH |
| AISI 52100 | — | 66.37 | — |
| CTAB | 1.99 | 25.6 | 20.38 |
| DI water | 2.48 | 26.1 | 21.18 |
| SLI | 4.02 | 28.54 | 23.66 |

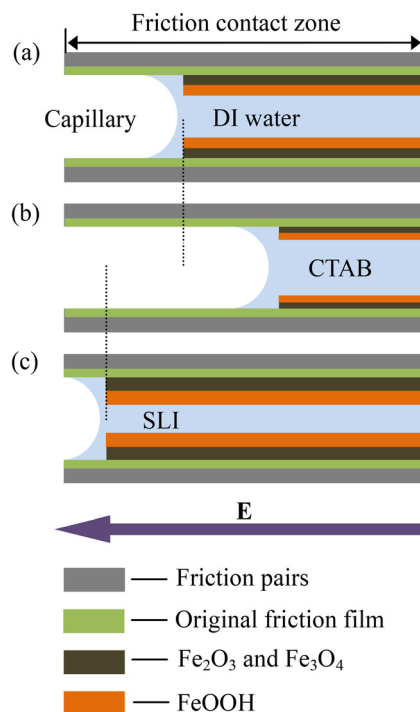


Fig. 11 Schematic of the lubricating layer under (a) DI water, (b) CTAB, and (c) SLI lubrication conditions.

the oxide film formed on the friction interfaces [54]. As shown in Fig. 11, the addition of SLI promoted the penetration of DI water into the capillary, which accelerated the formation of an oxide film on the contact interface, leading to the enhanced tribological performance of the steel-on-steel friction interface.

4 Conclusions

In this study, the EOF velocities of pure DI water, DI water with CTAB, and DI water with SLI in steel capillaries with different inner diameters were verified by measurements under different electric fields. The lubrication properties of these three types of lubricants were investigated by

four-ball experiments of a steel-on-steel sliding interfaces. The results showed that the tribological performance of these lubricants were related to their EOF velocities. Furthermore, the lubrication mechanism of DI water as the base lubricant added with an electroosmotic suppressant (CTAB) and an electroosmosis promoter (SLI) was also revealed. The conclusions obtained are as follows:

1) The penetration property of DI water in the capillaries can be modified by adding electroosmotic additives. In addition, the EOF velocity is directly proportional to the electric field intensity and inversely proportional to the inner diameter of the capillary.

2) Owing to the existence of one cationic group containing nitrogen and two carboxylic acid anion groups in one SLI molecule, the wall charges of the capillary doubled, resulting in a stronger EOF directed to the deeper contact region. With the increase in CTAB, the polarity of the wall charges was reversed (from "negative" to "positive") because of the adsorption of the quaternary ammonium cationic group in the CTAB on the negatively charged capillary wall; thus, the direction of EOF was finally reversed. In general, compared with pure DI water, the SLI lubricant can reduce the COF and WSD, whereas the CTAB lubricant exhibits an opposite behavior.

3) The rotational speed and applied load have great influences on the friction and wear performances because changes in the rotational speed and applied load can affect both the intensity of electron emission and inner diameter of the capillaries on the friction interface. The most significant difference in lubrication performance with different lubricants was observed when the rotating speed was 800 rpm and the applied load was 98 N.

4) The addition of SLI can promote lubricant penetration into the capillaries of the contact zone and is beneficial to form a thicker oxide layer on the friction interface. The friction contact is transformed from the original steel to steel into film to film, which reduces the COFs and WSDs.

In the next research, we plan to investigate the characteristics of EDLs and electron emission capacities of different friction interfaces in lubricants

to establish a capillary electroosmosis kinetic model of lubricants at friction interfaces.

Acknowledgements

The authors gratefully acknowledge the support of the National Natural Science Foundation of China (No. 51775507) and the Natural Science Foundation of Zhejiang Province (No. LY19E050006).

Open Access This article is licensed under a Creative Commons Attribution 4.0 International License, which permits use, sharing, adaptation, distribution and reproduction in any medium or format, as long as you give appropriate credit to the original author(s) and the source, provide a link to the Creative Commons licence, and indicate if changes were made.

The images or other third party material in this article are included in the article's Creative Commons licence, unless indicated otherwise in a credit line to the material. If material is not included in the article's Creative Commons licence and your intended use is not permitted by statutory regulation or exceeds the permitted use, you will need to obtain permission directly from the copyright holder.

To view a copy of this licence, visit <http://creativecommons.org/licenses/by/4.0/>.

References

- [1] Zhao J H, Yang G B, Zhang C L, Zhang Y J, Zhang S M, Zhang P Y. Synthesis of water-soluble Cu nanoparticles and evaluation of their tribological properties and thermal conductivity as a water-based additive. *Friction* 7(3): 246–259 (2019)
- [2] Godlevski V A, Volkov A V, Latyshev V N, Maurin L N. The kinetics of lubricant penetration action during machining. *Lubricat Sci* 9(2): 127–140 (1997)
- [3] Mane S, Joshi S S, Karagadde S, Kapoor S G. Modeling of variable friction and heat partition ratio at the chip-tool interface during orthogonal cutting of Ti-6Al-4V. *J Manuf Process* 55: 254–267 (2020)
- [4] Behera B C, Chetan, Setti D, Ghosh S, Rao P V. Spreadability studies of metal working fluids on tool surface and its impact on minimum amount cooling and lubrication turning. *J Mater Process Tech* 244: 1–16 (2017)

- [5] Hwang J. Direct observation of fluid action at the chip-tool interface in machining. *Int J Precis Eng Manuf* **15**(10): 2041–2049 (2014)
- [6] Hwang J, Chandrasekar S. Contact conditions at the chip-tool interface in machining. *Int J Precis Eng Manuf* **12**(2): 183–193 (2011)
- [7] Bierla A, Fromentin G, Minfray C, Martin J M, Le Mogne T, Genet N. Mechanical and physico-chemical study of sulfur additives effect in milling of high strength steel. *Wear* **286–287**: 116–123 (2012)
- [8] Zheng W J, Pei H J, Wang G C, Shen C G. A theoretical investigation on the capillary model of lubricant penetration. *Adv Mat Res* **383–390**: 3871–3875 (2011)
- [9] Liu J Y, Liu H P, Han R D, Wang Y. The study on lubrication action with water vapor as coolant and lubricant in cutting ANSI 304 stainless steel. *Int J Mach Tool Manuf* **50**(3): 260–269 (2010)
- [10] Xu X F, Feng B H, Huang S Q, Luan Z Q, Niu C C, Lin J B, Hu X D. Capillary penetration mechanism and machining characteristics of lubricant droplets in electrostatic minimum quantity lubrication (EMQL) grinding. *J Manuf Proc* **45**: 571–578 (2019)
- [11] Ciniero A, Le Rouzic J, Baikie I, Reddyhoff T. "The origins of triboemission-Correlating wear damage with electron emission". *Wear* **374–375**: 113–119 (2017)
- [12] Kharlamov V F. Effect of the electric field on electron chemi-emission from a semiconductor surface. *Tech Phys* **55**(6): 893–895 (2010)
- [13] Sokolowski-Tinten K, Ziegler W, von der Linde D, Siegal M P, Overmyer D L. Short-pulse-laser-induced optical damage and fracto-emission of amorphous, diamond-like carbon films. *Appl Phys Lett* **86**(12): 121911 (2005)
- [14] Banerjee A, Jiang C C, Lohiya L, Yang Y, Lu Y. Fracto-emission in lanthanum-based metallic glass microwires under quasi-static tensile loading. *J Appl Phys* **119**(15): 155102 (2016)
- [15] Wang W Q, Ji L, Li H X, Zhou H D, Ju P, Chen J M. Enhancing field electron emission behavior and mechanical properties of hydrogenated amorphous carbon films by incorporating vertically aligned carbon nanowires via facile reactive magnetron sputtering. *J Alloy Compd* **784**: 463–470 (2019)
- [16] Govindaraj J, Subbiah S. Charged-particle emissions during material deformation, failure and tribological interactions of machining. *J Tribol* **141**(3): 031101 (2019)
- [17] Nakayama K, Bou-Said B, Ikeda H. Tribo-electromagnetic phenomena of hydrogenated carbon films-Tribo-electrons, -ions, -photons, and -charging. *J Tribol* **119**(4): 764–768 (1997)
- [18] Nakayama K, Fujimoto T. The energy of electrons emitted from wearing solid surfaces. *Tribol Lett* **17**(1): 75–81 (2004)
- [19] Chiou Y C, Chang Y P, Lee R T. Tribo-electrification mechanism for self-mated metals in dry severe wear process: Part I. Pure hard metals. *Wear* **254**(7–8): 606–615 (2003)
- [20] Nakayama K, Nevshupa R A. Effect of dry air pressure on characteristics and patterns of tribomicroplasma. *Vacuum* **74**(1): 11–17 (2004)
- [21] Nakayama K, Nevshupa R A. Plasma generation in a gap around a sliding contact. *J Phys D Appl Phys* **35**(12): L53-L56 (2002)
- [22] Nakayama K. Mechanism of triboplasma generation in oil. *Tribol Lett* **41**(2): 345–351 (2011)
- [23] Ren C L, Li D Q. Improved understanding of the effect of electrical double layer on pressure-driven flow in microchannels. *Anal Chim Acta* **531**(1): 15–23 (2005)
- [24] Lee J, Moon H, Fowler J, Schoellhammer T, Kim C J. Electrowetting and electrowetting-on-dielectric for microscale liquid handling. *Sensor Actuat A Phys* **95**(2–3): 259–268 (2002)
- [25] van der Wouden E J, Heuser T, Hermes D C, Oosterbroek R E, Gardeniers J G E, van den Berg A. Field-effect control of electro-osmotic flow in microfluidic networks. *Colloid Surf A Physicochem Eng Aspects* **267**(1–3): 110–116 (2005)
- [26] Li L, Wang X Y, Pu Q S, Liu S R. Advancement of electroosmotic pump in microflow analysis. *Anal Chim Acta* **1060**: 1–16 (2019)
- [27] Sázelová P, Kasicka V, Koval D, Prusík Z, Fanali S, Aturki Z. Control of EOF in CE by different ways of application of radial electric field. *Electrophoresis* **28**(5): 756–766 (2007)
- [28] Razunguzwa T T, Timperman A T. Fabrication and characterization of a fritless microfabricated electroosmotic pump with reduced pH dependence. *Anal Chem* **76**(5): 1336–1341 (2004)
- [29] You H Y. *Electroosmosis and Its Application in Chromatography*. Beijing: Science Press, 2010.
- [30] Guan Q, Noblitt S D, Henry C S. Electrophoretic separations in poly(dimethylsiloxane) microchips using a mixture of ionic and zwitterionic surfactants. *Electrophoresis* **33**(2): 379–387 (2012)
- [31] Bekri S, Leclercq L, Cottet H. Influence of the ionic strength of acidic background electrolytes on the separation of proteins by capillary electrophoresis. *J Chromatogr A* **1432**: 145–151 (2016)
- [32] Chen L X, Ma J P, Guan Y F. An electroosmotic pump for packed capillary liquid chromatography. *Microchem J* **75**(1): 15–21 (2003)
- [33] Wang L, Wu J K. Flow behavior in microchannel made

- of different materials with wall slip velocity and electro-viscous effects. *Acta Mech Sin* **26**(1): 73–80 (2010)
- [34] Zhong W, Chen Y F. Hydrodynamic analysis of electroosmotic flow in micropump. *Chin J Mech Eng* **40**(2): 73–77 (2004)
- [35] Jiang C Y, Liu G, Zhang D H, Xu X P. Research on the microfluidics control method based on the EOF technology. *Mat Sci Forum* **532–533**: 65–68 (2006)
- [36] Huang S Q, Lv T, Wang M H, Xu X F. Enhanced machining performance and lubrication mechanism of electrostatic minimum quantity lubrication-EMQL milling process. *Int J Adv Manuf Tech* **94**(1–4): 655–666 (2018)
- [37] Huang S Q, Wang Z, Yao W Q, Xu X F. Tribological evaluation of contact-charged electrostatic spray lubrication as a new near-dry machining technique. *Tribol Int* **91**: 74–84 (2015)
- [38] Chen Y. *Capillary Electrophoresis Technology and Its Application*. Beijing: Chemical Industry, 2006
- [39] Brinksmeier E, Riemer O. Measurement of optical surfaces generated by diamond turning. *Int J Mach Tool Manu* **38**(5–6): 699–705 (1998)
- [40] Hu Z M, Dean T A. A study of surface topography, friction and lubricants in metalforming. *Int J Mach Tool Manuf* **40**(11): 1637–1649 (2000)
- [41] Jia D Z, Li C H, Zhang Y B, Yang M, Zhang X P, Li R Z, Ji H J. Experimental evaluation of surface topographies of NMQL grinding ZrO₂ ceramics combining multiangle ultrasonic vibration. *Int J Adv Manuf Tech* **100**(1–4): 457–473 (2019)
- [42] Nakayama K, Hashimoto H. Triboemission of charged particles and photons from wearing ceramic surfaces in various hydrocarbon gases. *Wear* **185**: 183–188 (1995)
- [43] Gáspár A, Gábor L. Study of quantitative analysis of traces in low-conductivity samples using capillary electrophoresis with electrokinetic injection. *J Chromatogr A* **1091**(1–2): 163–168 (2005)
- [44] Teixeira W S R, Santos M S F, Gruber J, Gutz I G R, Lopes F S. Determination of neutral diols and carboxylic acids formed during glycerol electrooxidation by capillary electrophoresis with dual (CD)-D-4. *Talanta* **178**: 1040–1045 (2018)
- [45] Wang W, Zhao L, Zhang J R, Zhu J J. Indirect amperometric measurement of electroosmotic flow rates and effective mobilities in microchip capillary electrophoresis. *J Chromatogr A* **1142**(2): 209–213 (2007)
- [46] Gao T, Li C H, Zhang Y B, Yang M, Jia D Z, Jin T, Hou Y L, Li R Z. Dispersing mechanism and tribological performance of vegetable oil-based CNT nanofluids with different surfactants. *Tribol Int* **131**: 51–63 (2019)
- [47] Tyle P, Frank S G. Penetration temperatures of aqueous sodium lauriminodipropionate solutions into solid phytosterols. *J Pharm Sci* **80**(2): 201 (1991)
- [48] Wojciechowski K, Linek K. Anion selectivity at the aqueous/polymeric membrane interface: A streaming current study of potentiometric Hofmeister effect. *Electrochim Acta* **71**: 159–165 (2012)
- [49] Huang S Q, Wang Z, Yao W Q, Xu X F. Tribological evaluation of contact-charged electrostatic spray lubrication as a new near-dry machining technique. *Tribol Int* **91**: 74–84 (2015)
- [50] Ferreira R O, Galvani G B, Tertuliano I S, Rodrigues A C P, Azevedo C R F. Characterization and evolution of the coefficient of friction during pin on disc tribotest: Comparison between C10200 Cu, AA6082-T6 Al and C36000 brass pins under varying normal loads. *Tribol Int* **138**: 403–414 (2019)
- [51] She D S, Yue W, Du Y J, Fu Z Q, Wang C B, Liu J J. Vacuum tribological properties of titanium with a nanocrystalline surface layer. *Tribol Lett* **57**(1): 1 (2015)
- [52] Yamashita T, Hayes P. Analysis of XPS spectra of Fe²⁺ and Fe³⁺ ions in oxide materials. *Appl Surf Sci* **254**(8): 2441–2449 (2008)
- [53] Liu J Y, Han R D, Zhang L, Guo H B. Study on lubricating characteristic and tool wear with water vapor as coolant and lubricant in green cutting. *Wear* **262**(3–4): 442–452 (2007)
- [54] Gao C P, Fan S G, Zhang S M, Zhang P Y, Wang Q H. Enhancement of tribofilm formation from water lubricated PEEK composites by copper nanowires. *Appl Surf Sci* **444**: 364–376 (2018)



Bohua FENG. He received his bachelor degree in mechanical engineering in 2016 from Zhijiang College of Zhejiang University of Technology, Hangzhou, China. Then, he is a Ph.D. student in the

Key Lab of Special Purpose Equipment and Advanced Manufacturing Technology, Ministry of Education & Zhejiang Province, Zhejiang University of Technology. His research interests include tribology, ultra precision machining, and green manufacturing technology.



Xuefeng XU. He received his M.S. degree in specialty of precision machinery and testing from Shanghai University of Science and Technology, China, in 1990. And he received his Ph.D. degree in mechanical and electronic engineering from Zhejiang University of Technology, China, in 2010. He has been engaged

in teaching and research in the field of mechanical manufacturing at Zhejiang University of Technology since 1992. His current position is a professor and the deputy director of the Key Lab of Special Purpose Equipment and Advanced Manufacturing Technology, Ministry of Education & Zhejiang Province. His research areas cover the tribology, green manufacturing technology, and precision and special processing technology.